Phase Diagrams of Alloys and Adsorbed Monolayers: Some Recent Results

B. Dünweg, S. Kämmerer, M. Presber
Institut für Physik, Universität Mainz, Postfach 3980
D–55099 Mainz, Germany

Abstract

We discuss some recent work done on the calculation of phase diagrams of models of binary alloys and adsorbed monolayers. For the nearest–neighbor Ising antiferromagnet on the fcc lattice (model for the Cu–Au system) we study a rather large lattice of 4×64^3 spins. This is necessary since the inherent frustration of the lattice induces a very small interfacial tension between ordered domains. We find no indications for the suggested L' phase, and locate the triple point at a *nonzero* temperature. There is some numerical evidence that it might in fact be a *multicritical* point. We then discuss the extension of lattice gas models to "elastic lattice gases" (ELGs) which include also translational degrees of freedom. Special attention is paid to the statistical treatment of vacant sites, and it is shown that a system A + vacancies is no longer equivalent to a system A + B. The ELG Hamiltonian is then studied for three–dimensional models on the diamond lattice for the unmixing of semiconductor alloys (where we find Mean–Field–like critical behavior), and for a two–dimensional model for $c(2 \times 2)$ structure formation.

1 Introduction: Lattice Gas and Ising Models

Although originally invented for magnetic systems, the Ising model is, in many cases, not a particularly good representation for real magnets, since its spin dimensionality $n = 1$ is too low. Conversely, it is very well suited to describe substitutional binary alloys (AB) or adsorbed monolayers, since in both cases there is a "pre–defined" lattice given by either the mixed crystal (three–dimensional alloy) or the adsorption sites of the substrate surface (two–dimensional adsorbate system), and there are two states per lattice site available (A–atom vs. B–atom in the alloy case, adsorbate atom vs. vacancy in the monolayer case). This analogy is made rigorous by the lattice gas model with pair interactions,

$$\begin{aligned} \mathcal{H}_{LG} &= -\sum_i \left\{ \varepsilon^A c_i + \varepsilon^B (1-c_i) \right\} \\ &+ \sum_{\langle ij \rangle} \left\{ v_{nn}^{AA} c_i c_j + v_{nn}^{AB} \left[c_i(1-c_j) + c_j(1-c_i) \right] + v_{nn}^{BB} (1-c_i)(1-c_j) \right\} \\ &+ \sum_{\langle\langle ij \rangle\rangle} \left\{ v_{nnn}^{AA} c_i c_j + v_{nnn}^{AB} \left[c_i(1-c_j) + c_j(1-c_i) \right] + v_{nnn}^{BB} (1-c_i)(1-c_j) \right\} + \ldots . \end{aligned} \tag{1}$$

Here, $c_i = 1$ if site i is occupied by an A–atom, while $c_i = 0$ otherwise (in the adsorbate case, B is just a vacancy). $\langle ij \rangle$ and $\langle\langle ij \rangle\rangle$ denote pairs of nearest and of next–nearest neighbors, respectively, and of course the model could also include interactions of even larger range. ε^A is the energy which is released upon placing an A–atom on a site, while v_{nn}^{AA} is the energy needed to build a nearest neighbor bond of two A–atoms. The other symbols' meaning is analogous. This Hamiltonian is quite general, and for an alloy one would specify $\varepsilon^A = \varepsilon^B = 0$, while for an adsorbate $\varepsilon^B = v_{\cdots}^{AB} = v_{\cdots}^{BB} = 0$.

Now this model is straightforwardly mapped onto an Ising model [1] by introducing the pseudospin variables $S_i = 2c_i - 1 = \pm 1$, and studying the model of N sites in the grand–canonical ensemble, whose partition function is

$$Z_{gc} = \sum_{N_A=0}^{N} \exp(\beta \mu_A N_A) \exp(\beta \mu_B N_B) Z_c(N_A), \tag{2}$$

where β is the inverse temperature $1/(k_B T)$, μ_A and μ_B denote the chemical potentials of species A and B, respectively (of course, $\mu_B = 0$ in the adsorbate case), and

$$Z_c(N_A) = \sum_{\{c_i\}|_{N_A}} \exp\left(-\beta \mathcal{H}_{LG}\right) \tag{3}$$

is the canonical partition function, the sum running over all configurations compatible with the constraint $\sum_i c_i = N_A$ (which automatically means $\sum_i (1 - c_i) = N_B = N - N_A$, such that in the alloy case one should use, strictly spoken, the term "semi–grand canonical ensemble"). With this transformation one finds, apart from an irrelevant prefactor

$$Z_{gc} = \sum_{\{S_i\}} \exp\left(-\beta \mathcal{H}_I\right) \tag{4}$$

with

$$\mathcal{H}_I = -J_{nn} \sum_{\langle ij \rangle} S_i S_j - J_{nnn} \sum_{\langle\langle ij \rangle\rangle} S_i S_j - \ldots - H \sum_i S_i \tag{5}$$

and

$$\begin{aligned} H &= \frac{1}{2}\left(\mu_A - \mu_B\right) + \frac{1}{2}\left(\varepsilon^A - \varepsilon^B\right) \\ &\quad - \frac{z_{nn}}{4}\left(v_{nn}^{AA} - v_{nn}^{BB}\right) - \frac{z_{nnn}}{4}\left(v_{nnn}^{AA} - v_{nnn}^{BB}\right) - \ldots, \end{aligned} \tag{6}$$

$$J_{nn} = \frac{1}{4}\left(2v_{nn}^{AB} - v_{nn}^{AA} - v_{nn}^{BB}\right), \tag{7}$$

$$J_{nnn} = \frac{1}{4}\left(2v_{nnn}^{AB} - v_{nnn}^{AA} - v_{nnn}^{BB}\right), \tag{8}$$

etc. Here z_{nn} and z_{nnn} denote the coordination numbers of the lattice in the nearest and next–nearest neighbor shell, respectively.

Though its apparent simplicity, $\mathcal{H}_I$ allows for a very rich physics. This is so because the model allows for competing interactions and resulting complicated antiferromagnetic structures. For a given set of J's, the usual Monte Carlo analysis of such a Hamiltonian proceeds as follows: (i) Find the ground states as a fuction of H; (ii) identify the phases, the pertinent order parameters (usually linear combinations of sublattice magnetizations), and their symmetry properties; (iii) from that, conclude the universality class of second–order transitions, if applicable (e. g. Ising, XY with cubic anisotropy, etc.); (iv) calculate

the phase diagram. This program looks rather straightforward, and in many cases it is. However, there are cases where the intrinsic complexity of $\mathcal{H}_I$ causes quite challenging problems, and one such case will be discussed in some detail in the next Section.

Nevertheless, despite these rather interesting properties, the above approach is clearly limited. One obvious deficiency is the symmetry of the resulting phase diagram: From the Ising symmetry (invariance of $\mathcal{H}_I$ with respect to $S_i \to -S_i$ and $H \to -H$), one concludes that the phase diagram in the grand–canonical ensemble (H–T plane) is symmetric around $H = 0$, while the corresponding canonical phase diagram (c–T plane, $0 \leq c \leq 1$ being the concentration of A–atoms) must be symmetric around $c = 0.5$. However, the phase diagrams of real systems are often strongly asymmetric, and the traditional approach to remedy this "sickness" has been to include also triplet interactions, i. e. terms $\propto S_i S_j S_k$.

However, this symmetry will also be destroyed as soon as the model also includes *elastic* interactions, i. e. explicitly takes into account the translational degrees of freedom of each particle. Moreover, this modification also changes the *range of the effective interaction* between the spins *qualitatively* because two spins, although being located rather far away from each other, nevertheless interact with each other due to the long–range elastic distortions of the lattice. For this reason, these systems are also of fundamental physical interest, since the universal critical behavior of second–order phase transitions may well be affected. The rest of this contribution will therefore discuss some recent studies of such models. Sec. 3 will be devoted to the modeling and the related methodological problems, while Sec. 4 and 5 discuss the application to a three–dimensional model for a mixture of Si and Ge (note that the effects of elastic interactions, i. e. most notably the atomic size mismatch, are expected to be most pronounced in covalently bonded systems like semiconductor alloys), and to a two–dimensional model for an adsorbed monolayer of hydrogen on a palladium (100) surface, respectively.

2 The Nearest–Neighbor Ising Antiferromagnet on the FCC Lattice

We study the Hamiltonian of Eqn. 5 on the fcc lattice for the case $J = J_{nn} < 0$, while all other exchange couplings vanish, and we limit ourselves to $H > 0$ for symmetry reasons. A physical realization of this system is the alloy Cu_xAu_{1-x}, i. e. in this system the same ordered superstructures occur [2]. The phase diagram of this model has been the subject of a long–standing debate, and calculations have been done, with ever–increasing accuracy, using the Mean Field approximation or Kikuchi's cluster variation method (CVM) [3–9], low–temperature expansions [10–12] and Monte Carlo (MC) simulations [13–20, 9]. The present MC study [21, 22] is the most expensive simulation of the system so far, and has attempted to resolve the controversial issues about the location of the triple point and about the existence of the L' phase (see below).

The reason why this system has been so hard to analyze is the geometric *frustration* of the fcc lattice: It is impossible to assign spins to a nearest–neighbor tetrahedron such that all six bonds are antiferromagnetic. Therefore, the ground state [23] does not exhibit three–dimensional order but only two–dimensional order (except for $H > 12|J|$, where all spins are up), i. e. it is a sequence of perfectly ordered (either ferromagnetic or antiferromagnetic) (100) planes. Every antiferromagnetic plane yields a twofold degeneracy (since it may be shifted freely in itself), such that the ground state is macroscopically degenerate

with nevertheless vanishing entropy. For $H < 4|J|$, all planes are antiferromagnetic, while for $4|J| < H < 12|J|$ every second plane is ferromagnetic. At the "superdegenerate" point $H = 4|J|$ the ground state entropy is nonzero.

For $T > 0$, three–dimensional order becomes *entropically* stabilized [10–12], since the ordered phases AB ($H < 4|J|$) and A_3B ($4|J| < H < 12|J|$) admit more low–energy excitations than a disordered ground state. As usual, a configuration of two ordered domains separated by two interfaces (also called antiphase boundaries, APBs; note the periodic boundary conditions) costs a free energy penalty of $\Delta F = 2\sigma L^2$, where L is the linear system size and σ the interfacial tension [24]. However, the pathology is that σ has a purely entropic origin, and hence vanishes quickly upon $T \to 0$. For this reason, L must be rather large in order to make ΔF sufficiently large, and practical tests [21] showed that we needed an $N = 4 \times L^3$ system with $L = 64$, while $L = 32$ still showed some tendency towards APBs, and $L = 16$, which had been used in older studies [13–15], is clearly too small.

In order to describe the ordered phases, we decompose the system into four interpenetrating simple cubic sublattices (a, b, c, d), and introduce

$$\begin{aligned} \psi_0 &= (m_a + m_b + m_c + m_d)/4 \\ \psi_1 &= (m_a + m_b - m_c - m_d)/4 \\ \psi_2 &= (m_a - m_b + m_c - m_d)/4 \\ \psi_3 &= (-m_a + m_b + m_c - m_d)/4, \end{aligned} \tag{9}$$

where m_α are the sublattice magnetizations varying between -1 and $+1$. ψ_0 is the total magnetization, and ψ_1, ψ_2 and ψ_3 are the components of the three–dimensional order parameter $\vec{\psi}$, which vanishes in the disordered phase where all sublattices are equivalent. The perfectly ordered AB state is then given by two sublattices with $S_i = +1$, the other two sublattices having magnetization -1. Likewise, in the A_3B state only one sublattice has magnetization -1, all the other spins being $S_i = +1$. The AB phase is hence described by the six states $\vec{\psi} = (\pm\psi_{AB}, 0, 0)$, $(0, \pm\psi_{AB}, 0)$ and $(0, 0, \pm\psi_{AB})$, and the A_3B phase by the four states $\vec{\psi} = (\psi_{A3B}, \psi_{A3B}, \psi_{A3B})$, $(\psi_{A3B}, -\psi_{A3B}, -\psi_{A3B})$, $(-\psi_{A3B}, \psi_{A3B}, -\psi_{A3B})$, $(-\psi_{A3B}, -\psi_{A3B}, \psi_{A3B})$, where $|\psi_{AB}| < 1$ and $|\psi_{A3B}| < 1/2$ describe states which are not perfectly ordered. The so–called L' phase corresponds to *three* different sublattice magnetizations (ideally, two sublattices up, one down, and one with random spin orientation); this phase has been found stable by CVM calculations in the vicinity of $H = 4|J|$ [7]. We carefully searched for this phase at various state points by starting the system in a perfect L' state, and monitoring the time evolution of the sublattice magnetizations. In all cases, the system ended up in an AB or A_3B state, and hence we believe that this phase is an artifact of the CVM.

Similarly, the old MC studies [13–15] had suggested that the triple point, where AB, A_3B and the disordered phase coexist, should occur at $H = 4|J|$, $T = 0$. We hence looked, in a similar fashion, also for stability of the disordered phase near $H = 4|J|$ at low temperatures, with the same result, i. e. evolution into an AB or A_3B state. Therefore, the triple point must occur at a *nonzero* temperature. We then mapped out the phase boundaries, using standard hysteresis loops and thermodynamic integration to find intersecting branches of the free energy F, using the relations $N\psi_0 = -\partial F/\partial H$ and $U = -T^2\partial(F/T)/\partial T$ for the internal energy.

Note that all transition lines are expected to be of first order: The six states of the AB

phase correspond to a Heisenberg model with cubic anisotropy, whose transition into the disordered phase has been shown to be first–order by renormalization–group arguments [25]. Similarly, the A_3B phase corresponds to a 4–state Potts model (relevant for the transition into the disordered phase), while the transition from A_3B to AB corresponds to a 3–state Potts model (note that one out of three sublattices must be flipped) [26].

Our results are summarized in Fig. 1. One sees that the data indeed confirm the anticipated first–order behavior of all three transition lines, and the triple point is located at $k_B T_t/|J| = 0.98 \pm 0.02$, $H_t/|J| = 3.60 \pm 0.04$. Moreover, we find that all first–order jumps along all three lines get very small when approaching the triple point. We hence believe that this point might actually be a *multicritical* point, such that the jumps would tend to *zero*. Indeed, our order parameter data along the AB $\leftrightarrow$ A_3B transition line are well compatible with tricritical scaling. However, our resolution is not fine enough to unambiguously answer this subtle question; this would require further large–scale simulations of even significantly larger lattices. We believe that an accurate finite–size scaling analysis would prove very difficult, due to the high order parameter dimensionality, and the very large minimum system size which is necessary. It should also be noted that a multicritical point is *not* predicted by Landau theory [22].

3 Inclusion of Elastic Interactions

The "fundamental" approach to a classical simulation of an alloy or adsorbate system with continuous degrees of freedom would consist in the specification of an interatomic potential (depending on distances, bond angles, atomic species, ...) and, for modeling the influence of a substrate, an external potential. The particles would then freely move around, and, depending on the current geometric configuration, find the neighbors with which they interact. One could also introduce a grand–canonical ensemble via particle creation and destruction, or a semi–grand canonical description via changes A $\leftrightarrow$ B. Indeed, for fluids, this approach *must* be used, and has recently been applied to rather accurate studies of the gas–liquid transition of two– and three–dimensional Lennard–Jones systems [27, 28].

However, it is also obvious that such a model is computationally rather cumbersome: Each particle's neighbor shell fluctuates and must be continuously checked and updated. We have hence chosen to deliberately neglect these fluctuations and instead study a two– or three–dimensional *network* with the same *topology* as the original lattice. Since this topology is conserved during the simulation, one can use the same neighbor list for the interactions once and for all, such that from the point of view of data structures the simulation is as efficient as a simple lattice simulation. Actually, the types of Hamiltonians we are interested in are directly related to the original lattice gas, Eqn. 1: One simply has to replace the interaction parameters v_{nn}^{AA} etc. by distance–depending functions,

$$v_{nn}^{AA} \rightarrow v_{nn}^{AA}\left(|\vec{r}_i - \vec{r}_j|\right) \tag{10}$$

(similarly the other v's), and the adsorption energies ε^A, ε^B by functions depending on the particle's distance from its ideal adsorption site:

$$\varepsilon^A \rightarrow \varepsilon^A\left(\left|\vec{r}_i - \vec{r}_i^{\,id}\right|\right). \tag{11}$$

Again, for describing an alloy one would specify $\varepsilon^A = \varepsilon^B = 0$, while in the adsorbate case $\varepsilon^B = v_{\cdots}^{AB} = v_{\cdots}^{BB} = 0$. The resulting Hamiltonian shall be denoted with $\mathcal{H}_{ELG}$ ("elastic lattice gas").

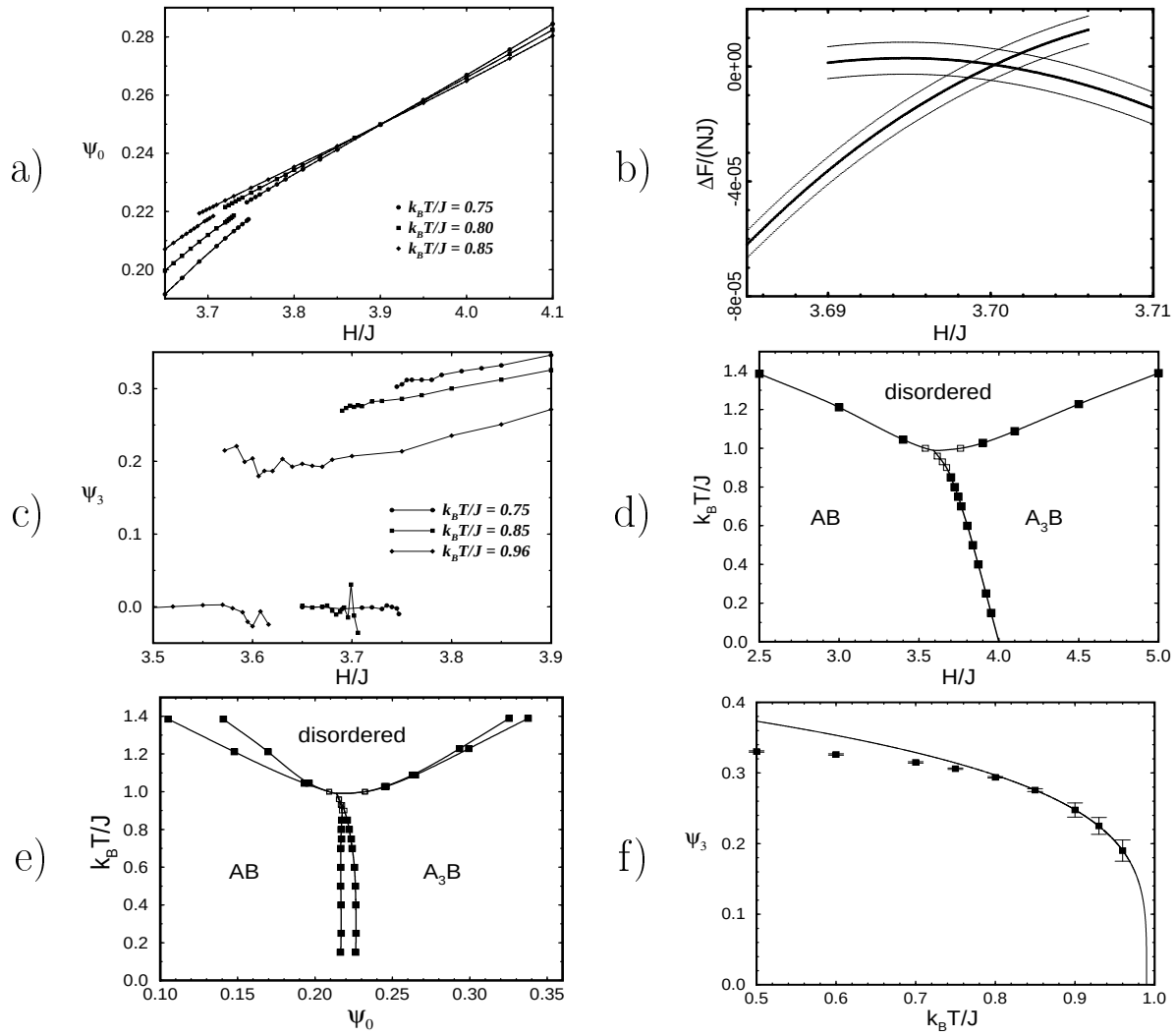

Figure 1: (From Ref. [22]) *a)* Total magnetization as function of field, for temperatures as indicated. Hysteresis indicates the first–order nature of the transition AB $\leftrightarrow$ A_3B. *b)* Branches of the free energy per site as function of field, at temperature $k_BT = 0.85|J|$, resulting from a cubic spline fit to the magnetization data and thermodynamic integration. Errors in the individual data points were estimated via standard MC error analysis, while the error in the free energy was estimated via standard error propagation. For sake of clarity of the plot, a "background" contribution linear in H has been subtracted. *c)* Hysteresis loops of order parameter component ψ_3, which vanishes in the simulated AB state, while it is nonzero in the A_3B phase. The first–order jumps decrease strongly upon approaching the triple point. *d)* Phase diagram in the grand–canonical ensemble. Filled symbols have been obtained by thermodynamic integration, open symbols by direct inspection of order parameter hystereses. *e)* Phase diagram in the canonical ensemble. *f)* Order parameter component ψ_3, evaluated along the AB $\leftrightarrow$ A_3B coexistence line, as a function of temperature. The line represents a fit $\psi_3 \propto (T_t - T)^{\beta_t}$ with $k_BT_t = 0.99|J|$ and $\beta_t = 0.2416$, while tricritical scaling would imply $\beta_t = 1/4$. However, every exponent in the range $0.2 \ldots 0.3$ is compatible with the data.

Of course, such a simplified Hamiltonian loses some of the physics which could otherwise be modeled by the translational degrees of freedom, since both structural phase transitions as well as melting are explicitly excluded. However, sufficiently far away from such transitions we expect the model to describe the physics reasonably well.

This model has a number of peculiarities which shall now be discussed. First of all, one should note that the particles should be considered as *distinguishable*: Each particle can be uniquely identified by its position on the network, and hence prefactors $(N_A!)^{-1}$, $(N_B!)^{-1}$ do *not* occur in the partition function. Moreover, the model's "philosophy" is to assign *independent* degrees of freedom c_i and $\vec{r}_i$ to each lattice site i, and to also update these degrees of freedom independently of each other in the grand–canonical ensemble. However, if the B–particle is a vacancy, this assignment is unphysical and artificial, since physically it does not make sense to ask for the coordinate of a non–existent particle. Nevertheless, this assignment is useful in order to facilitate a compact and straightforward simulation algorithm. This is the reason why the transformation to the grand–canonical ensemble is no longer as straightforward as before, and why the systems A + B (alloy) and A + vacancies (adsorbate) *are no longer equivalent* [29].

Let us now discuss the transformation to the grand–canonical ensemble in some more detail. Eqn. 2 is of course still valid, but Z_c must now also include the translational degrees of freedom of the *real* particles. To make this more explicit, consider the lattice sites as enumerated from 1 to N. A given configuration $\{c_i\}$ can then be associated in a unique way with indices $i_1 < i_2 < \ldots < i_{N_A}$ and $j_1 < j_2 < \ldots < j_{N_B}$ such that $c_{i_k} = 1$ and $c_{j_k} = 0$. Moreover, we introduce the numbers $\chi_{nn}(i,j) = 1$ if i and j are nearest neighbors, and zero otherwise, and similarly $\chi_{nnn}(i,j)$ for next–nearest neighbors, etc. $\mathcal{H}_{ELG}$ can then be rewritten as

$$\begin{aligned}
\mathcal{H}_{ELG} &= -\sum_{k=1}^{N_A} \varepsilon^A\left(\left|\vec{r}_{i_k} - \vec{r}^{\,id}_{i_k}\right|\right) - \sum_{k=1}^{N_B} \varepsilon^B\left(\left|\vec{r}_{j_k} - \vec{r}^{\,id}_{j_k}\right|\right) \\
&+ \sum_{1\le k<l\le N_A} \chi_{nn}(i_k,i_l) v_{nn}^{AA}\left(|\vec{r}_{i_k} - \vec{r}_{i_l}|\right) \\
&+ \sum_{k=1}^{N_A}\sum_{l=1}^{N_B} \chi_{nn}(i_k,j_l) v_{nn}^{AB}\left(|\vec{r}_{i_k} - \vec{r}_{j_l}|\right) \\
&+ \sum_{1\le k<l\le N_B} \chi_{nn}(j_k,j_l) v_{nn}^{BB}\left(|\vec{r}_{j_k} - \vec{r}_{j_l}|\right) \\
&+ \ldots,
\end{aligned} \tag{12}$$

where the next–nearest neighbor and higher contributions are written in the same way as the nearest neighbor terms. In the alloy case we then find for the canonical partition function, using an arbitrary normalization volume V_0,

$$\begin{aligned}
Z_c^{alloy}(N_A) &= \sum_{\{c_i\}|_{N_A}} V_0^{-N_A} V_0^{-N_B} \int d\vec{r}_{i_1} \ldots \int d\vec{r}_{i_{N_A}} \times \\
&\quad \times \int d\vec{r}_{j_1} \ldots \int d\vec{r}_{j_{N_B}} \exp\left(-\beta \mathcal{H}_{ELG}\left(\{\vec{r}_{i_k}\},\{\vec{r}_{j_l}\}\right)\right) \\
&= \sum_{\{c_i\}|_{N_A}} V_0^{-N} \int d\vec{r}_1 \ldots \int d\vec{r}_N \exp\left(-\beta \mathcal{H}_{ELG}\left(\{c_i\},\{\vec{r}_i\}\right)\right),
\end{aligned} \tag{13}$$

such that, apart from a constant prefactor,

$$Z_{gc}^{alloy} = \sum_{\{c_i\}} V_0^{-N} \int d\vec{r}_1 \ldots \int d\vec{r}_N \exp\left(-\beta \mathcal{H}_{eff}\left(\{c_i\}, \{\vec{r}_i\}\right)\right) \tag{14}$$

with

$$\mathcal{H}_{eff} = \mathcal{H}_{ELG} - (\mu_A - \mu_B) \sum_i c_i. \tag{15}$$

I. e. in this case the same transformation as in the simple lattice gas case applies. $\mathcal{H}_{eff}$ can, of course, be used directly to control a standard Metropolis algorithm. In the adsorbate case with vacancies, however, only the coordinates of the *real* particles appear:

$$Z_c^{adsorb}(N_A) = \sum_{\{c_i\}|_{N_A}} V_0^{-N_A} \int d\vec{r}_{i_1} \ldots \int d\vec{r}_{i_{N_A}} \exp\left(-\beta \mathcal{H}_{ELG}\left(\{\vec{r}_{i_k}\}\right)\right). \tag{16}$$

We now construct an effective Hamiltonian $\mathcal{H}_{eff}$ by *requiring* that the grand–canonical partition function Z_{gc}^{adsorb} can also be written in the form of Eqn. 14. Then $\mathcal{H}_{eff}$ can be used directly for a standard Metropolis scheme, too. We start with the *ansatz* [29]

$$\mathcal{H}_{eff} = \mathcal{H}_{ELG} - (\mu_A + \alpha k_B T) \sum_i c_i + \sum_i (1 - c_i) U_0 \left(\left|\vec{r}_i - \vec{r}_i^{id}\right|\right). \tag{17}$$

The physical motivation is that without the counterterms $\alpha > 0$, $U_0 \geq 0$ particle destruction processes become more and more likely with increasing temperature and increasing system size, for entropical reasons: The ghost particles can explore the full system volume, while the real particles are confined to their immediate neighborhood. The purpose of U_0 is to confine also the ghost particles around their adsorption sites, while the term α provides for the necessary temperature dependence (for higher temperatures, the creation of real particles becomes more and more favored by this term). Inserting Eqn. 17 into Eqn. 14, one finds, after splitting the integration into real coordinates $\vec{r}_{i_k}$ and ghost particle coordinates $\vec{r}_{j_l}$,

$$Z_{gc}^{adsorb} = \sum_{N_A=0}^{N} \exp\left(\beta \mu_A N_A\right) \exp\left(N_A \alpha + N_B \ln \zeta\right) Z_c^{adsorb}(N_A), \tag{18}$$

where we have introduced the single–particle partition function resulting from the potential U_0,

$$\zeta = V_0^{-1} \int d\vec{r} \exp\left(-\beta U_0(\vec{r})\right). \tag{19}$$

Obviously, a correct simulation algorithm is obtained for $\alpha = \ln \zeta$ (note $\mu_B = 0$). We have tested [29] two choices of U_0, (i) $U_0 = 0$, i. e. $\alpha = \ln(V/V_0)$, where V is the total system volume, and (ii) a square–well potential which confines the particle to a volume V_c, i. e. $\alpha = \ln(V_c/V_0)$. It turned out that only the second choice is useful, for purely *dynamic* reasons: If no confining potential is used, the ghost particles are free to travel through all of the system. However, as soon as they are some lattice constants away from their ideal site, a rematerialization would place them onto a very high energy level, due to the strong potential ε^A (for which we used a harmonic spring). Hence, this rematerialization is forbidden by the Boltzmann factor, and does not occur until the random walker happens to come close to its ideal site again. The correlation time

of the algorithm should be roughly proportional to the time needed for these "loops", and this should, from diffusion arguments, scale like L^2 if L is the linear system size. I. e. this algorithm has intrinsic critical slowing down built in, independent of the state point! The square–well potential obviously removes this problem, while, per construction, it nevertheless yields correct static averages. Note also that the arbitrary normalization parameter V_0 enters the simulation algorithm. This means that the chemical potential μ_A is only defined after V_0 has been specified, i. e. a change of V_0 corresponds to a temperature–dependent redefinition of the zero of μ_A. Hence, for such simulations the μ_A–T phase diagram needs the additional specification of V_0.

One also sees rather easily that the Ising symmetry will in general no longer hold for the ELG: After transforming to pseudospin variables, the Hamiltonian assumes the form

$$\mathcal{H} = \mathcal{H}_0\left(\{\vec{r}_i\}\right) - \sum_{\langle ij \rangle} J_{ij}\left(\{\vec{r}_i\}\right) S_i S_j - \sum_{\langle\langle ij \rangle\rangle} J_{ij}\left(\{\vec{r}_i\}\right) S_i S_j - \ldots - \sum_i H_i\left(\{\vec{r}_i\}\right) S_i, \qquad (20)$$

and it is impossible to induce a change $H_i \to -H_i$ via just changing the chemical potential (note also that for the so–called "compressible Ising model" [30] $H_i \equiv 0$). Hence, we do not view the Ising language as particularly useful for the ELG. For adsorbed monolayers, the "elastic" route towards phase diagram asymmetries has already qualitatively been noted by Persson [31].

4 The Si–Ge Unmixing Transition

For a binary alloy of silicon and germanium, we studied an ELG on the diamond lattice. Apart from nearest–neighbor pair interactions, we also introduced three–body interactions. This was *not* done in order to induce a phase diagram asymmetry, but rather in order to stabilize the fourfold coordinated structure of the diamond lattice, i. e. the tetrahedron angle. The first simulation [32] used the Keating potential [33]:

$$v_{nn}^{\alpha\beta}(r) = \phi_{nn}^{\alpha\beta} + E^{\alpha\beta}\left[r^2 - \left(l_0^{\alpha\beta}\right)^2\right]^2 \qquad (21)$$

with $\alpha, \beta \in \{A, B\}$. The corresponding three–body term is

$$v_3^{\alpha\beta\gamma} = A^{\alpha\beta\gamma}\left[\vec{r}_{ij} \cdot \vec{r}_{kj} + \frac{1}{3} l_0^{\alpha\beta} l_0^{\gamma\beta}\right]^2, \qquad (22)$$

i. e. the summation runs over all angles with vertex at site j, occupied with species β (note $\cos\Theta_t = 1/3$ for the tetrahedron angle Θ_t). For the interaction parameters, see Ref. [32]. This model was simulated at constant vanishing pressure [34] in order to accomodate the atomic size mismatch, for systems of up to $N = 8 \times 10^3$ sites. The unmixing phase diagram was calculated using thermodynamic integration procedures [32].

The critical behavior of the model was analyzed by a multi–histogram analysis [35] of data taken near the critical point. The results are shown in Fig. 2. First, we calculated the fourth–order cumulant of the (extensive) magnetization (in Ising language),

$$U_4 = 1 - \frac{\left\langle \left(M - \langle M \rangle\right)^4 \right\rangle}{3\left\langle \left(M - \langle M \rangle\right)^2 \right\rangle^2}, \qquad (23)$$

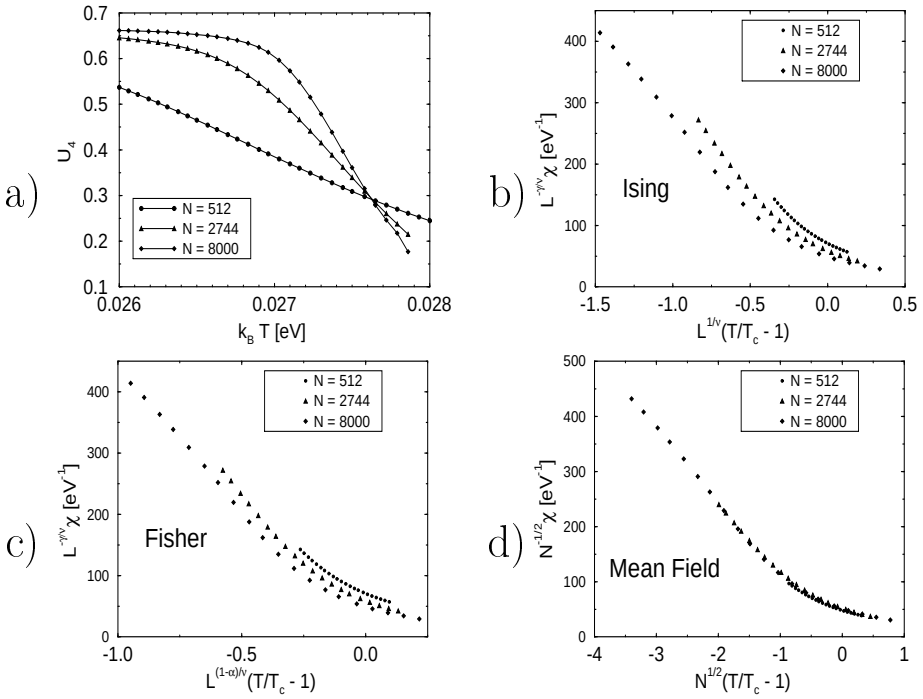

Figure 2: (From Ref. [32]) Critical behavior of the ELG modeling a Si–Ge alloy using the Keating potential: *a)* Maximum value of the cumulant as a function of temperature, for three system sizes as indicated. *b)* Data collapsing plot for the susceptibility, checking for Ising–like critical behavior. *c)* Same as b) for Fisher–renormalized exponents. *d)* Same as b) for Mean Field critical behavior.

as a function of both chemical potential and temperature and determined, at fixed temperature, its maximum, the location defining the critical chemical potential. Plotting the resulting values as a function of temperature yields Fig. 2 a), showing that the standard cumulant intersection method for an accurate determination of the critical point works also for the ELG.

The finite–size scaling relation for the susceptibility reads in the Ising case

$$\chi = (Nk_BT)^{-1}\left(\left\langle M^2\right\rangle - \langle M\rangle^2\right) \tag{24}$$

$$\chi = L^{\gamma/\nu}\tilde{\chi}\left(tL^{1/\nu}\right), \tag{25}$$

with $t = T/T_c - 1$, $\gamma = 1.24$, $\nu = 0.63$, while for Fisher–renormalized exponents [36] (which are not expected in the present case) one has to replace $\gamma \to \gamma_{eff} = \gamma/(1-\alpha)$, $\nu \to \nu_{eff} = \nu/(1-\alpha)$ with $\alpha = 0.12$. In the Mean Field case one has [37]

$$\chi = L^{d/2}\tilde{\chi}\left(tL^{d/2}\right). \tag{26}$$

As seen from Fig. 2 b)–d), the data are in best agreement with Mean Field critical behavior. This is probably due to an effective long–range interaction induced by the elastic distortions. It is expected that this corresponds to a dipolar interaction, for which the upper critical dimension is $d = 3$ [38].

It should be mentioned that a similar study [39] was also done for the Stillinger–Weber (SW) potential [40]. The same Mean–Field–like behavior was found; however, the SW

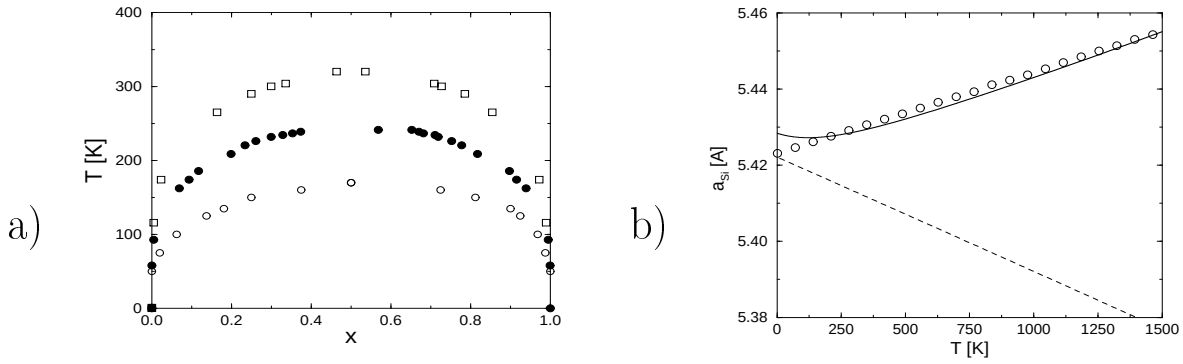

Figure 3: (From Ref. [39]) *a)* Unmixing phase diagram of $Si_{1-x}Ge_x$ alloys using different models: Keating potential [32] (open squares), SW potential [39] (solid circles), Tersoff potential [41]. This latter potential is even significantly more complicated, and the critical behavior had not been studied in this paper. *b)* Lattice constant of pure Si as a function of temperature, for Keating potential (dashed line), SW potential (open circles), and fit to experiments (solid line).

potential yields a different critical temperature, and a more physical behavior of thermal expansion, see Fig. 3. For more details, see Refs. [32, 39].

5 Hydrogen on Pd(100)

We used a simple two–dimensional ELG (adsorbate and vacancies) on the square lattice to model, e. g., the adsorption of H on Pd, taking into account both nearest as well as next–nearest neighbor interactions [29]. The Hamiltonian is specified via simple harmonic springs,

$$\varepsilon^A(r) = \frac{k_0}{2} r^2 \tag{27}$$

$$v_{nn}^{AA}(r) = \phi_{nn} + \frac{k_{nn}}{2} \left(r - l_{nn}\right)^2 \tag{28}$$

and

$$v_{nnn}^{AA}(r) = \phi_{nnn} + \frac{k_{nnn}}{2} \left(r - l_{nnn}\right)^2 \tag{29}$$

where the lattice constant is set to unity, and the springs' rest lengths are, for simplicity, assumed to be fully compatible with the substrate lattice, $l_{nn} = 1$ and $l_{nnn} = \sqrt{2}$. We choose $\phi_{nn} = +4$ and $\phi_{nnn} = -4$ in dimensionless units, and, for simplicity, $k_0 = k_{nn} = k_{nnn} = 1$. The ghost particles were confined to circular areas of unit radius around the ideal adsorption sites (cf. Eqn. 17). Likewise, we set the normalization volume V_0, which defines the chemical potential for $T > 0$, to $V_0 = 1$.

For $k_i = 0$ the model reduces to a LG whose properties had been studied a long time ago [42]. The phase diagram's topology (see Fig. 4) is unchanged by the elastic effects. There occurs just one ordered structure, $c(2 \times 2)$, i. e. a nearest–neighbor antiferromagnet (cf. Fig. 5), whose transition to the disordered phase is of second order for high temperatures, while it is of first order for low temperatures. Interestingly enough, the overall

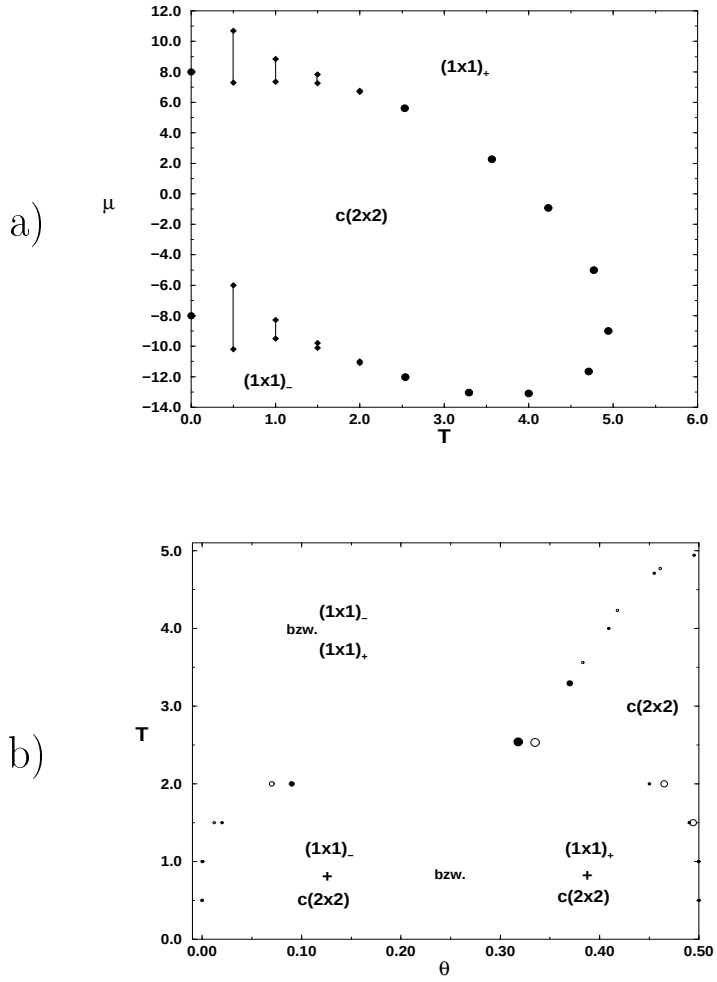

Figure 4: (From Ref. [29]) *a)* Phase diagram of the two–dimensional model specified in Eqns. 27–29, in the grand–canonical ensemble. The asymmetry is not surprising, in view of the chemical potential for $T > 0$ being unique only up the normalization volume V_0 (cf. Sec. 3). Solid circles denote second–order transitions, while diamonds denote hysteresis ranges of first–order transitions. *b)* Phase diagram of the same model in the canonical ensemble; $0 \leq \Theta \leq 1$ is the coverage. Solid circles, $0 \leq \Theta \leq 0.5$; open circles, $0.5 \leq \Theta \leq 1$. Data for Θ and $1 - \Theta$ have been included in the same figure in order to make the weak asymmetry more visible. Errors are always of the order of symbol sizes.

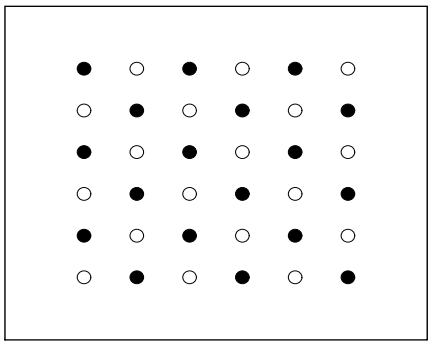

Figure 5: (From Ref. [29]) The $c(2 \times 2)$ structure.

asymmetry of the canonical phase diagram is rather weak. Moreover, the overall shape is only weakly changed in comparison with the pure LG [42].

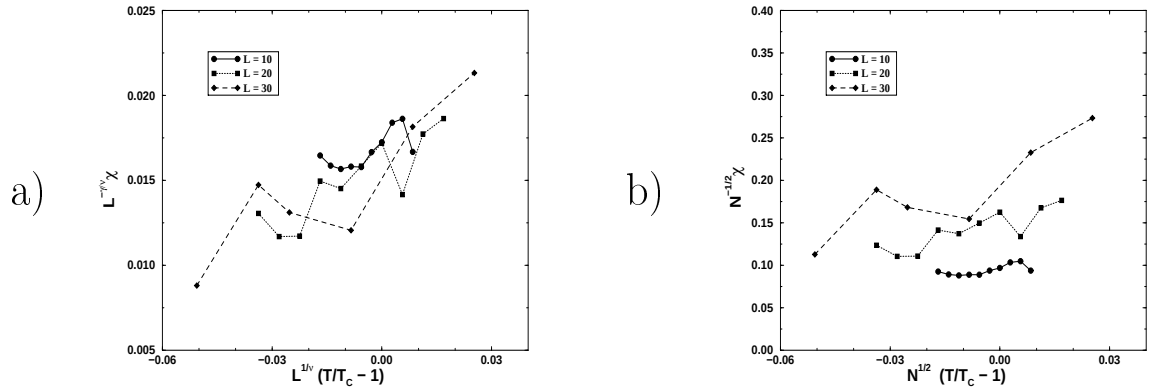

Figure 6: (From Ref. [29]) *a)* Data collapsing plot of the staggered susceptibility for 2d Ising exponents, at $T_c = 4.231$. *b)* Same as a) for Mean field behavior.

The second–order phase transitions were analyzed by standard finite–size scaling of the susceptibility of the staggered magnetization, i. e. the difference in sublattice magnetizations of the two sublattices separated by nearest–neighbor bonds, using system sizes $L = 10, 20, 30$. The data are not accurate enough to draw firm conclusions, but it seems that they are in better agreement with Ising–like behavior than with Mean Field, see Fig. 6. This would further corroborate the hypothesis that the upper critical dimension is $d = 3$ for the ELG.

Acknowledgements

The work reported here was done in close collaboration with D. P. Landau, K. Binder, M. Laradji, and M. d'Onorio de Meo. B. D. also gratefully acknowledges support from the Alexander von Humboldt foundation, and from a NATO travel grant.

References

[1] K. Binder, in *Adv. Sol. State Physics*, edited by P. Grosse (Vieweg, Braunschweig, 1986), Vol. 26, pp. 133–168.

[2] F. Ducastelle, *Order and Phase Stability in Alloys* (North Holland, Amsterdam, 1991).

[3] W. Shockley, J. Chem. Phys. **6**, 130 (1938).

[4] U. Gahn, Z. Metallkunde **64**, 268 (1973).

[5] R. Kikuchi, J. Chem. Phys. **60**, 1071 (1974).

[6] J. M. Sanchez, D. de Fontaine, and W. Teitler, Phys. Rev. B **26**, 1465 (1982).

[7] A. Finel and F. Ducastelle, Europhys. Lett. **1**, 135 (erratum 543) (1986).

[8] A. Finel, in *Alloy Phase Stability*, edited by G. M. Stocks and A. Gonis (Kluwer, Dordrecht, 1989), pp. 269–280.

[9] R. Tetot, A. Finel, and F. Ducastelle, J. Stat. Phys. **61**, 121 (1990).

[10] J. Slawny, J. Stat. Phys. **20**, 711 (1979).

[11] J. Slawny, in *Phase Transitions and Critical Phenomena*, edited by C. Domb and J. L. Lebowitz (Academic Press, London, 1987), Vol. 11, pp. 127–205.

[12] J. Bricmont and J. Slawny, J. Stat. Phys. **54**, 89 (1989).

[13] K. Binder, Phys. Rev. Lett. **45**, 811 (1980).

[14] K. Binder, Z. Phys. B **45**, 61 (1981).

[15] K. Binder, J. L. Lebowitz, M. K. Phani, and M. H. Kalos, Acta Metall. **29**, 1655 (1981).

[16] U. Gahn, J. Phys. Chem. Solids **43**, 977 (1982).

[17] U. Gahn, J. Phys. Chem. Solids **47**, 1153 (1986).

[18] H. Ackermann, S. Crusius, and G. Inden, Acta Metall. **34**, 2311 (1986).

[19] H. T. Diep, A. Ghazali, B. Benge, and P. Lallemand, Europhys. Lett. **2**, 603 (1986).

[20] J. L. Lebowitz, M. K. Phani, and D. F. Styer, J. Stat. Phys. **38**, 413 (1985).

[21] S. Kämmerer, Diplom thesis, Johannes Gutenberg–Universität Mainz, 1994.

[22] S. Kämmerer, B. Dünweg, K. Binder, and M. d'Onorio de Meo, Phys. Rev. B **53**, 2345 (1996).

[23] O. J. Heilmann, J. Phys. A **13**, 263 (1980).

[24] K. Binder, Z. Phys. **B 43**, 119 (1981).